A Coarse-Grained Model for Polyphenylene Dendrimers: Switching and Backfolding of Planar Three-Fold Core Dendrimers

Paola Carbone,*,† Fabrizia Negri,‡ and Florian Müller-Plathe†

Technische Universität Darmstadt, Petersenstrasse 20, D-64287 Darmstadt, Germany, and Dipartimento di Chimica "G. Ciamician", Università di Bologna, Via F.Selmi 2, 40126 Bologna, Italy

Received May 2, 2007; Revised Manuscript Received June 27, 2007

ABSTRACT: In this paper, we present a mesoscopic model for melt of polyphenylene dendrimers. The coarse-graining force field is built on the basis of the distribution functions derived from atomistic simulations, and thus it takes into account the chemical details of the system. Owing to the reduced number of particles, simulations of melts longer than 0.1 μs for dendrimer generation up to the fourth have been carried out to investigate both bulk and single molecule properties. In the bulk, it has been shown that these dendrimers do not acquire orientational order. Single molecule geometrical analysis has been performed by computing the radius of gyration, hydrodynamic radius, and small-angle neutron scattering profile. All the computed parameters compare favorably with experimental data and with previous atomistic simulations. It is concluded, in agreement with previous atomistic studies, that polyphenylene dendrimers present a substantially rigid structure that does not allowed for a remarkable back-folding even in the melt phase. Interestingly, the switching between a collapsed and open global shape found in previously isolated-molecule atomistic simulations occurs also in the melt phase.

1. Introduction

Dendrimers are a special class of branched polymers characterized by a multifunctional core from which relatively short chains (called branches or dendrons) emanate. Each branch end is characterized by a specific functional group which, reacting with another "monomer", builds the new generation. The use of several chemical groups to functionalize the chain ends and the nearly full control over the synthetic process make this class of macromolecules suitable for the design of novel nanostructured materials and for several possible applications.[1] The perfectly branched, monodisperse structure of dendrimers makes them valuable model compounds for studying fundamental electrochemical[2] and photophysical processes,[3] and, depending on their chemical structure, they can be important building blocks of supramolecular chemistry.[4] Several applications have been proposed for dendrimers, and in all cases the flexibility of the dendrons plays a fundamental role. The understanding of the molecular structure of dendrimers in solution or bulk represents one of the most important prerequisites for their controlled designed. Particular attention has to be devoted to the end group distribution within the dendrimer molecule, the intramolecular conformational changes and their time scale, the intermolecular packing and the presence and accessibility of intra- and inter dendrimer cavities.

A new class of dendritic systems, composed only of carbon and hydrogen atoms, has been recently synthesized.[5] Starting from polyfunctional central building blocks, a generation-by-generation buildup of structurally defined, highly branched polyphenylene dendrimers (PDs) has become possible.[6,7] Among other uses, these dendrimers are employed as precursors in the synthesis of well-defined polycyclic aromatic hydrocarbons (PAHs), from which more complex supramolecular structures, such as liquid crystals, can be obtained.[8,9] Due to their semirigid framework and very dense intramolecular packing, the monodisperse PDs are of interest with respect to the controlled design of shape-invariant nanoparticles.[10]

Several theoretical approaches are used to describe dendrimers, explaining at the molecular scale the macroscopically observed properties,[11] and most of them, not surprisingly, are similar to those used in polymer physics. They include the following: (i) analytical or continuum methods focused on finding principles of universality, in some well-defined limit, that permit the general description of the system regardless of the microscopic details;[12] (ii) computational methods on simplified systems that describe dendrimer systems with a specific shape and topology but without chemical details;[13] (iii) computational methods at the atomistic level. Of the latter type Brownian dynamics (BD),[14] Monte Carlo (MC),[15] and molecular dynamics (MD)[16] simulations are intensively used. The inclusion of the chemical details in the simulation of dendrimer solutions or melts costs in term of computer time because the system size easily exceeds 20 000 atoms. Despite this, a considerable number of atomistic MD simulations were carried out on different dendrimers in dilute solutions, but only one on the amorphous bulk state.[17] A useful compromise for a computational study of dendrimers would be a coarse-grained model which reduces the degrees of freedom of the system, while taking into account the chemical identity. No attempt has yet been made in this direction, to the best of our knowledge. In view of the polymeric nature of dendrimers, a coarse-grained model, as for polymers, is the natural choice. Recently, a method to adjust coarse-grained force fields to a specific system on various length scales has been developed. These mesoscale models have been applied to a large variety polymers with very good results.[18] They reproduce very well the structural properties of the melt; moreover, a suitable back-mapping procedure permits to reintroduce the atomistic details into the model, in order to obtain relaxed melts of high molecular weight polymers.[19−21] Using such a method, long time molecular dynamics simulations on dilute solutions and amorphous bulks of high-generation dendrimers should be feasible.

* Corresponding author. E-mail: p.carbone@theo.chemie.tu-darmstadt.de.
† Technische Universität Darmstadt.
‡ Dipartimento di Chimica "G. Ciamician", Università di Bologna.

10.1021/ma071001f CCC: $37.00
Published on Web 08/16/2007

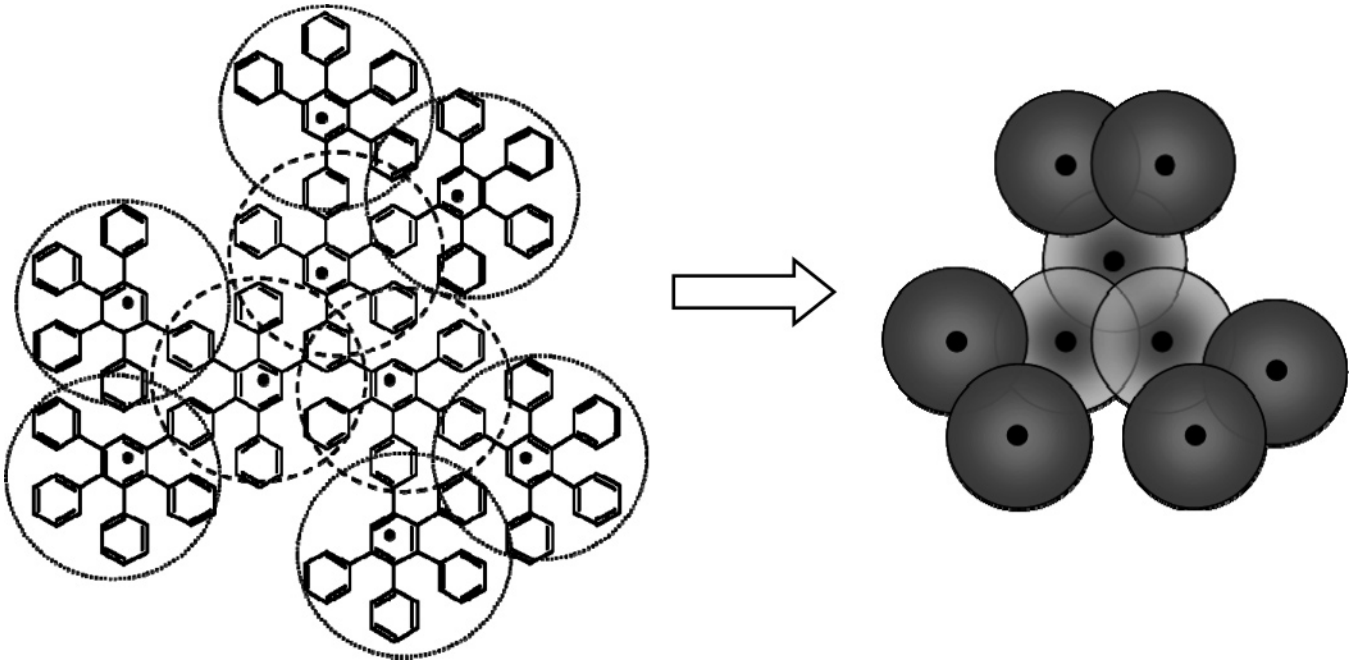

Figure 1. Atomistic and coarse-grained representation of the first and second generation of polyphenylene dendrimer. The black points represent the center of mass of the beads. On the left side of the arrow, the dashed and dotted circles correspond respectively to beads of type A and type B.

Recently, molecular mechanics and molecular dynamics calculations have been reported to study the nature of stable conformers and the shape persistence of monodisperse PDs based on different cores.[22−24] In particular extended molecular dynamics (MD) investigations studied the shape persistence of isolated polyphenylene dendrimers of first (G1) and second (G2) generation with a planar core formed by a 1,3,5-trisubstituted benzene ring (Figure 1). These allowed us to make a general classification of the conformations assumed by the three dendrimer branches with respect to the planar core.[24] These studies found a direct correlation among the dendrimer core conformations and the global shape of the dendrimers, and proved that, depending on the temperature, the G2 dendrimers oscillate between two global shape states: *open* and *collapsed*. The MD simulations show that at 80 K G1 and G2 dendrimers conserve their initial shape for several nanoseconds, while, at room temperature for the G2, a reversible oscillation among two states occurs. The presence of this "switching" and a structural characterization of higher generation of PDs in the melt phase can be conveniently studied via coarse-grained simulations.

In this paper, we develop a coarse-grained model for PDs in the melt phase. The coarse-grained force field is built up starting from atomistic simulations (employing the same force field of ref 24) of a bulk system of G2 PDs so that it implicitly takes into account the chemical details of the system. We show the results of several coarse-grained molecular dynamics (CG-MD) simulations of melts of PDs from generation 2 until generation 4 (G4), performed for times longer than 0.1 μs. Particular attention is paid to the analysis of the conformation and general shape of individual molecules in the bulk environment compared with the results found for the isolated molecule and with the available experimental data.

2. Coarse-Grained Model and Mesoscopic Force Field Development

The rigidity of the system and the approximate sphericity of the subunits allow us to collect the atoms in beads of quite large dimension, compared to typical coarse-graining schemes for linear polymers. In Figure 1, a schematic representation of the mapping scheme is depicted. As the only relevant degrees of freedom involve the bonds connecting the tetrasubstituted phenyl rings, the natural choice is to define a bead, which contains the entire repeat unit, placed at the center of mass. In this way, only one type of bead (called A) is necessary to build the model for the G1 dendrimers, while for the G2 two bead types (the inner one is again of type A and the outer one is called B) are used. To develop the force field for the coarse-grained model, we follow the procedure detailed in previous papers.[19,25] Here, we only summarize the main steps. From the atomistic simulations of G2 PDs the probability distributions of the two types of bond (A−A and A−B) and of the three different types of angles (A−A−A, B−A−B, and B−A−A) are obtained, and subsequently fitted with a suitable number of Gaussian functions (see Figure 2). The bond and angle distributions are then Boltzmann-inverted to give the coarse-grained potential energy functions for these interactions.[19] In Tables 1 and 2, the Gaussian parameters for bond and angle types are reported. Moving from the second generation to higher generations the number of bond types becomes three (A−A, A−B, and B−B) and a further angle type (B−B−B) is needed.

Because of the comparable chemical structure of the beads A and B and to the high symmetry of the coarse-grained structure, we use for the new bonds (B−B) the same parameters as for the A−B stretching and for the angle B−B−B the parameters B−A−B. As in other cases, torsional interactions have been omitted, while the nonbonded interactions have been parametrized using iterative Boltzmann inversion starting from the atomistic radial distribution functions. The G2 dendrimers present three (A−A, A−B, and B−B) types of nonbonded interactions. The potentials of mean force ($F(r)$) for these interactions have been obtained by Boltzmann inverting the corresponding target radial distribution functions from atomistic simulations (RDF_{target}).

$$F(r) = -k_B T \ln RDF_{target}(r)$$

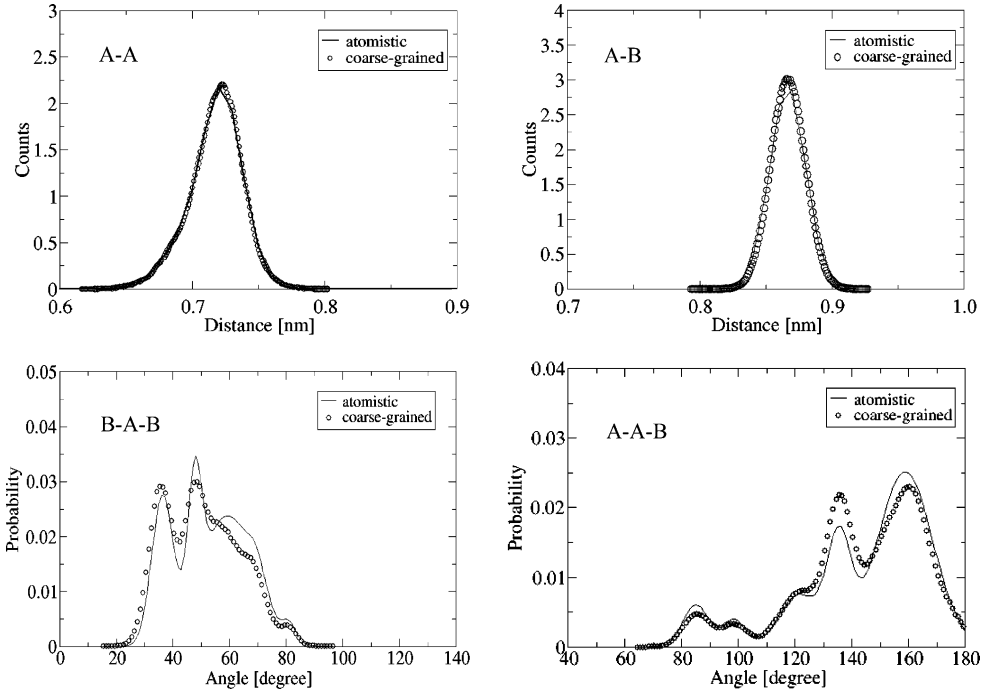

Figure 2. Histogram of A−A and A−B bond lengths (top part), and bending angles B−A−B and A−A−B (bottom part), of second generation dendrimers extracted from atomistic (solid line) and coarse-grained (dashed line) simulations.

Table 1. Gaussian Parameters for the Bond Distribution for $P(r) = \sum_{i=1}^{n} A_i/w_i\sqrt{\pi/2}\ \exp(-2(r - l_i)^2/w_i^2)$

		G2			
bond type	n	i	A_i	w_i [nm]	l_i [nm]
A−A	2	1	0.64	0.062	0.708
		2	0.32	0.028	0.725
A−B; B−B	1	1	1.00	0.023	0.866

Table 2. Gaussian Parameters for the Angle Distribution for $P(\theta) = \sum_{i=1}^{n} A_i/w_i\ \sqrt{\pi/2}\ \exp(-2(\theta - \theta_i)^2/w_i^2)$

		G2			
angle type	n	i	A_i	w_i [deg]	θ_i [deg]
A−A−A	3	1	0.76	7.5	58.3
		2	0.48	3.9	61.4
		3	0.04	2.2	67.4
B−A−B; B−B−B	5	1	0.11	7.6	36.22
		2	0.07	4.7	47.8
		3	0.68	19.5	59.3
		4	0.09	5.7	69.6
		5	0.04	4.4	81.1
A−A−B	5	1	0.11	9.0	85.0
		2	0.04	8.42	98.4
		3	0.16	8.48	135.4
		4	0.46	19.5	158.8
		5	0.12	13.7	121.3

These free energies cannot be used directly as potentials because they already contain the cooperative many-body effects arising from the packing of particles in material. However, they can be used as initial guesses $V_0(r)$ in an iteration process, which modifies the potential of mean force to obtain the effective nonbonded potentials.

$$V_{i+1}(r) = V_i(r) + k_B T \ln \frac{\mathrm{RDF}_i(r)}{\mathrm{RDF}_{\mathrm{target}}(r)}$$

The tabulated numerical potentials are iterated until they yield the target RDFs from the atomistic reference simulations. In practice, a small number of MD simulations at constant temperature and density conditions (for the details, see the computation details section) are necessary to converge the coarse-grained RDFs to the corresponding target RDFs.

This mapping scheme leads to beads of large radius (∼0.66 nm), and the corresponding RDFs are rather complicated. After a few iterations, however, convergence is reached and the force field reproduces satisfactorily the target RDFs; moreover, the pressure is quite close to the target one (∼18 atm instead of 1 atm). To remove this small discrepancy in the pressure, we reoptimize the system by adding to the potential a weak linear potential term $\Delta V(r) = A(1 - r/r_{\mathrm{cutoff}})$ to the attractive long range part of $V_i(r)$. The pressure optimization, after a few cycles, gives a final pressure of 0.99 atm.

Figure 3 shows the comparison among intermolecular pair correlation functions coming from the atomistic simulations (solid line) and those obtained with the coarse-grained models (empty circles). All pair interactions are in acceptable agreement with the target RDF, even if small discrepancies are evident. The inconsistency in the A−A interaction (Figure 3a), where the CG RDF is always below the atomistic RDF, is only an apparent one. This effect arises from the peculiar 3D-symmetry of dendrimers in contrast with linear polymer chains. Beads of type A are firmly located inside the dendrimer scaffold, and in the coarse-grain representation they are partially shielded from interactions with other molecules by beads of type B ("cage effect"). Moreover, the A−A nonbonded potential coming from the corresponding inverted RDF, is purely repulsive, so that the beads repel each others. The resulting coarse-grained RDF A−A is actually dominated to a large extent by A−B and B−B interactions, rather than A−A interactions. As a result it lies always below the target RDF within the cutoff radius (<1.6 nm), to which the plot extends. For distances bigger than the cutoff radius, the coarse-grained RDF exceeds the corresponding atomistic one, giving the same total number of particles (not shown).

3. Computational Details

MD Atomistic Simulations. The atomistic MD simulations are carried out on the bulk of second generation PDs. The rigidity of

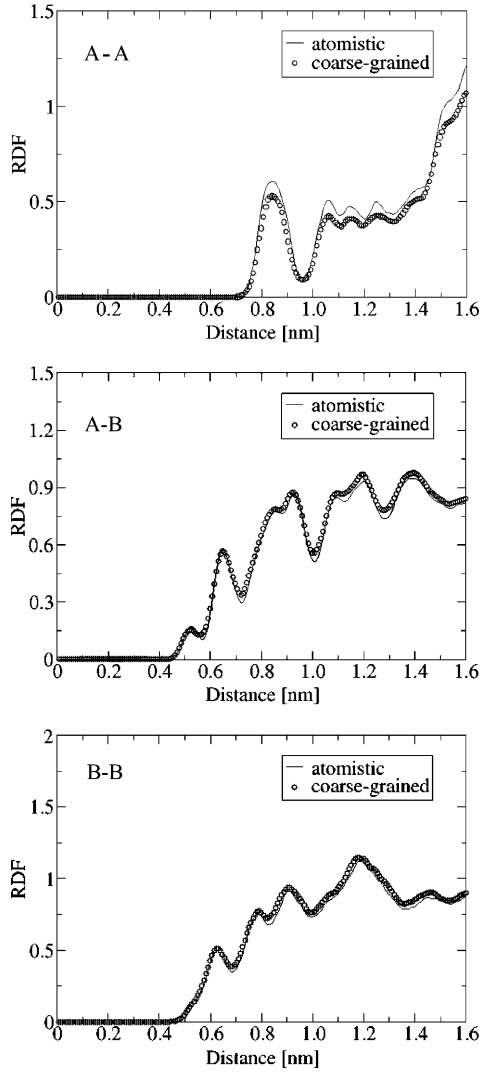

Figure 3. Radial distribution functions of second-generation dendrimer (intermolecular part only). Continuous lines: atomistic RDFs for the three different pair interactions (A−A, A−B, and B−B). Empty circles: RDFs obtained from the last iteration of the Boltzmann inversion scheme.

the PDs makes the preparation of the simulation box quite easy in comparison with flexible polymer chains: eight dendrimers, separately minimized in vacuum, are put, in a random orientation, in a box corresponding to a density of 0.7 g/cm^3 to avoid the overlaps between the atoms. After that, a minimization and subsequently a sequence of NVT simulations (300 ps each) are applied to relax the system and, reducing gradually the volume, until a density of ∼1 g/cm^3 is reached. The production runs are carried out under NPT controlled pressure and temperature conditions using the periodic boundary conditions until the systems reach the equilibrium density.

A coupling Berendsen thermostat and barostat with respective coupling times $\tau_T = 0.1$ ps (the same was used in the NVT equilibration runs) and $\tau_P = 2.0$ ps are used to keep the temperature and the pressure close to the desired values. For the pressure this value is 1atm, the temperature is fixed at 323 K. The time step used is 1 fs and the production runs are 8 ns long; the van der Waals interactions are truncated beyond 1.2 nm. All the simulations are carried out with the TINKER software[26] using the MM3 empirical potential which is particularly well suited to describe conjugated systems owing to its explicit description of the π-system.[27] The final density is 0.89 g/cm^3.

Coarse-Grained MD Simulation. The coarse-grained force field is developed and optimized on a system of eight coarse-grained G2 dendrimers. The molecules are put in a simulation box with orthorhombic periodic boundary conditions; the simulations are performed using the GMQ_num code, a version of the GMQ package[28] able to handle numerical potential. The density achieved during the optimization is 0.92 g/cm^3, in agreement with the one obtained from the atomistic simulations.

Table 3. Details of the Systems under Investigation

				density [g/cm^3]	
generation	no. of atoms	no. of beads	CG sim length [ns]	atomistic	CG
G2	462	9	100	0.89	0.92[a]/1.00[b]
G3	1062	21	100	-	1.20[b]
G4	2162	45	100	-	1.16[b]

[a] Density obtained from NPT simulations performed on eight PDs. [b] Density obtained from the production runs with 216 PDs.

The production runs are performed using a simulation box containing 216 molecules of PDs of second, third (G3), or fourth (G4) generations respectively. We could not generate starting structures of fifth generation molecules because of the steric crowding at the chain ends. This limit in the generation degree is in agreement with the incomplete conversion that occurs during the synthesis for generations higher than four.[29]

The simulations are carried on at constant temperature (323 K) and constant pressure (1 atm). The time constants for the Berendsen thermostat and barostat are set to 0.15 and 5 ps. The time step is 10 fs and cutoff radius for the nonbonded interaction is set to 1.6 nm.

The density values found for the G2, G3, and G4 dendrimers after 100 ns of production run in the NPT ensemble are 1.0, 1.20, and 1.16 g/cm^3 respectively.

It should be noticed that with 216 molecules of G2 PDs, the density of the system is slightly larger than that observed with 8 molecules. Such difference does not show up in the corresponding RDFs. This increase in density can be explained with better packing possibilities due to the presence of more molecules. This effect seems not to occur for the bigger generations: for both G3 and G4 identical density values are obtained from the CG simulations of 8 or 216 molecules.

In Table 3, the number of atoms and the corresponding number of beads, the coarse-grained and atomistic density values and the length of the CG simulations are reported for all systems investigated.

4. Results

Bulk Properties: Free Volume Analysis and Order Tensor Calculation. From the pioneering work of Fox and Flory[30] it is known that the density of a bulk of linear polymer chains depends on the number of monomers per chain and this dependence is caused by the extra free volume of the chain ends. In particular the density increases with polymer chain length (up to a certain limit) because the effect of the free volume of the chain ends is reduced increasing the molecular weight. Several computational studies have investigated the influence of the end-monomer free volume on static and dynamics properties of melts of unentangled linear chains.[31] As far as we know, no similar systematic analysis has been performed on dendrimer melts. Here the number of the end-monomer increases with the generation and the relation for the linear chain is not valid. There can be several reasons for the generation dependence of the density in dendrimers melts: (i) the effect of the free volume of the chain ends, (ii) the change of the intradendrimer free volume with the generation, and (iii) the different intermolecular packing that changes with the generation. Looking at the free volume of the monomer ends, it can be argued that the role played by them in the density depends on the flexibility of the dendrimer branch. The extra free volume per chain end, responsible for the increase of the density in linear

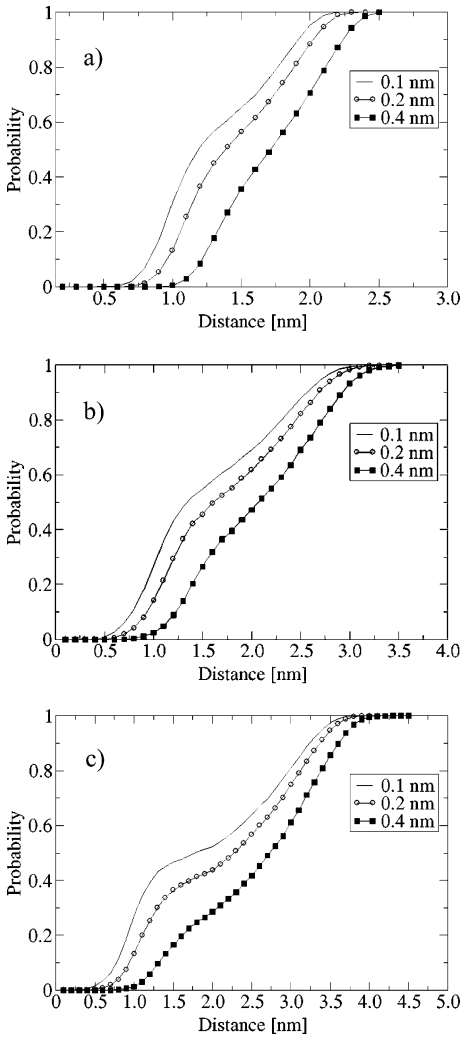

Figure 4. Free volume calculation inside the polyphenylene dendrimer scaffold for different probe dimensions. The three plots correspond to different dendrimer generation: (a) second-generation, (b) third-generation, and (c) fourth-generation.

polymer, can be drastically reduced when the branches are so flexible that the monomer ends lie inside the dendrimer scaffold close to its core. As we are going to show later, in the present case, the PD structure is quite stiff and we expect that all the chain ends reside outside the molecule. On the basis of this assumption, we expect that the density decreases with the generation. In contrast, we have an increase between G2 and G3 and a slightly decrease when we move to G4. This finding favors the second or the third hypothesis cited above. To check the internal free volume of the coarse-grained dendrimers, we use the random particle insertion method with probes of different size. Figure 4 shows the internal free volume (expressed as a probability of finding free volume for a probe randomly placed within the dendrimer normalized with respect to the total number of insertions) as a function of the distance from the dendrimer center of mass.

From Figure 4, it is clear that the free volume captured inside the dendrimer has the same trend for all generations. Because of the stiffness of the PD scaffold, the free volume increases from the core to the end monomers almost monotonically. These results bring us to think that the reason for the density trend with the PD generation lies in the intermolecular packing, but further investigations are needed to clarify this behavior.

There are no experimental values for the bulk density of PDs but, looking at the experimental values for poly(propylenimine) functionalized and unfuctionalized, reported by Tande et al.,[32] it is clear that the trend of the density value is not easy to predict. Since the change in density as a function of branch flexibility and generation is fundamental for understanding the bulk properties of dendrimers, a more systematically analysis will be carried out in future studies. All following results correspond to simulations carried out on 216 molecules, unless noted otherwise.

Beyond the molecular rigidity another interesting behavior of PDs is their ability to self-assemble. Experiments on PDs deposited on graphite shows that the PDs spontaneously form a monolayer on the basal plane. Moreover, complex supramolecular structures, such as rods or two-dimensional crystals, were imaged with atomic force microscopy.[33] The self-assembly behavior is induced by the graphite surface. In this contribution, we want to investigate, by the inspection of the order tensor and the orientational autocorrelation function, if also in the three-dimensional bulk the peculiar chemical structure of the PDs induces any order. In this way, we also monitor the efficiency of the coarse-grained model in the global relaxation of the dendrimers.

The order tensor is defined as

$$\mathbf{S} = \frac{3}{2}\left\langle \frac{1}{N}\sum_{i=1}^{N} \mathbf{u}_i \otimes \mathbf{u}_i - \frac{1}{3}\mathbf{I} \right\rangle$$

where the unit vector $\mathbf{u}_i$ denotes the direction of the molecule i, and it is the eigenvector corresponding to the smallest eigenvalue of the inertia tensor of the same molecule i. In the formula $\mathbf{I}$ is the unit tensor and N is the number of molecules in the simulation box. The average is computed over the all molecules and the angle brackets denote the average over the trajectory. The largest eigenvalue of the order tensor is called the order parameter τ and it indicates if the molecules are oriented along the same direction ($\tau = 1$) or not ($\tau = 0$). For all generations, we obtain a value of τ around zero showing that there is no favorite orientation of the molecules in the box.

To check the global relaxation of the dendrimers we calculate the orientation correlation function, defined as

$$P_2(t) = \frac{1}{2}\langle 3[\mathbf{v}(t)\cdot\mathbf{v}(0)]^2 - 1\rangle$$

where $\mathbf{v}$ is the unit vector connecting the dendrimer center of mass and one of the end beads, and the average is over the trajectory and the molecules.

In Figure 5, the P_2 calculated for one G4 PD molecule (the slowest system) is depicted: the function goes to zero within 15 ns, showing the perfect relaxation of the system. The curve can be fitted to the stretched exponential (Kohlrausch−Williams−Watts) functional form (Figure 5):

$$P_2(t) = \exp(-(t/\tau_{KWW})^{\beta})$$

The corresponding relaxation time τ is the integral of the exponential function. We find $\tau \sim 840$ ps. This shows that, orientationally, the molecules are relaxed in the 100 ns simulation time. This would have been impossible to achieve with an atomistic model.

Single Molecule Characterization: Gyration Tensor and Shape Anisotropy. In a previous publication,[24] we analyzed in detail the three-dimensional structure of isolated G1 and G2 PDs focusing on the dynamical evolution of the conformations assumed by the core of the dendrimer and the associated dendrimer global shape. This analysis was mainly carried out

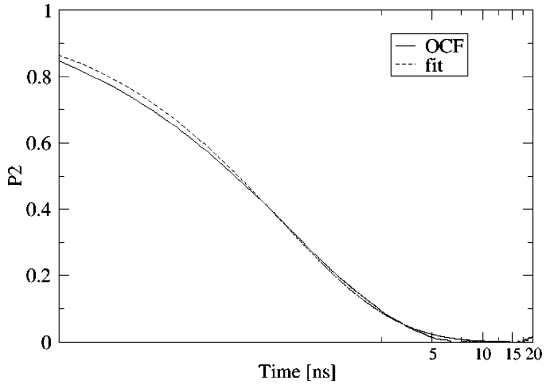

Figure 5. Orientational autocorrelation function (OCF) P_2 (see text) of a individual polyphenylene dendrimer of generation fourth averaged over all 216 molecules (solid line) and its fitting to the Kohlrausch−Williams−Watts equation (dot line).

by the calculation of the second moment of the atomic distribution (the gyration tensor) which is defined as (assuming uniform masses)

$$\mathbf{R}_{\alpha,\beta}{}^2 = \frac{1}{N}\sum_{i=1}^{N}(\mathbf{r}_\alpha{}^i - \mathbf{r}_\alpha{}^M)(\mathbf{r}_\beta{}^i - \mathbf{r}_\beta{}^M) \quad \alpha,\beta = x, y, z$$

where N is the number of atoms in the PD, $\mathbf{r}_\alpha^i$ is the position of the ith atom and $\mathbf{r}_\alpha^M$ is the position of the dendrimer's geometrical center. The eigenvalues of the gyration tensor ($\lambda_1{}^2$, $\lambda_2{}^2$, and $\lambda_3{}^2$) represent the characteristic lengths of the equivalent ellipsoid with which the dendrimer is described.

The characteristic lengths can be combined to give several parameters describing the distribution of the particles: the most used is the squared radius of gyration $R_g{}^2$ which is defined as the trace of the tensor.

$$R_g{}^2 = I_1 = \mathrm{tr}(\mathbf{R}^2) = \lambda_1{}^2 + \lambda_2{}^2 + \lambda_3{}^2$$

Another important parameter is the relative shape anisotropy k^2 defined as

$$k^2 = 1 - \frac{3I_2}{I_1{}^2}$$

where I_2 is the second invariant of $\mathbf{R}^2$ defined as

$$I_2 = \lambda_1{}^2{\cdot}\lambda_2{}^2 + \lambda_2{}^2{\cdot}\lambda_3{}^2 + \lambda_3{}^2{\cdot}\lambda_1{}^2$$

The value of k^2 ranges between 0 and 1. A linear array of atoms (i.e., a rigid-rod molecule), for example, is characterized by k^2=1; for a homogeneously filled polygon $k^2 = {}^1/_4$; for structures with tetrahedral or high 3-d symmetry, k^2=0.

In previous atomistic MD simulations,[24] we observed that isolated G2 PDs showed an interesting switching among two well-defined global conformations, and, looking at the time evolution of the characteristic lengths (λ_i), we were able to follow this transition. Moreover the change in shape could be visualized and related to the core conformation of the dendrimers. Atomistic simulations of bulk systems did not show any of these shape changes and, apart from small geometrical changes, the initial conformations were maintained during the entire simulation length (the coarse-grained force field used in this paper has been developed starting from the distributions obtained from these atomistic simulations). This observation can be explained in two ways: PDs in the bulk state behave differently from PDs in vacuum, or the simulation time window (8 ns) is too short. The coarse-grained model described in section 2 is able to address this issue. The same geometrical characterization, with the calculation of the shape anisotropy factor, has been done for the coarse-grained PD in all generations.

We will show that, although the coarse-grained potential was built starting from the atomistic bulk simulation, the coarse-grained model produces the same switching which was observed in the atomistic gas phase. As in the atomistic case, it is possible to follow the conformational changes by monitoring the eigenvalues λ_i and to visualize the two typical shapes; however, there is, of course, no information about the dendrimer core conformations.

Figure 6 (top part) shows the time evolution of the largest λ_i for G2 along 7 ns of the trajectory with the corresponding 3D pictures of the *open* and *collapsed* structures. The main signature of these structures is the ratio among the two λ_i and the bottom part of Figure 6 shows its distribution. The distribution can be fitted using two Gaussian functions center in 0.3 and 0.4. In this case it is hard to say that the distribution is bimodal (as it will be evident for the higher generations). This is due to the approximation that the CG model, using spherical beads, makes in describing the dendrimer shape (see Table 4 third and fourth columns), which results more discoid (λ_2 and λ_3 are similar) than in the atomistic description.

Not surprisingly, the rate of the conformational jumps in the coarse-grained simulation is greater than in the atomistic ones (in which case the dendrimer is even in vacuum). It is already known that the dynamics in a coarse-grained system is accelerated with respect to the corresponding atomistic system.[34] The reason lies in the nature of the coarse-grained force field: inversion of the RDF leads to a softer repulsion and a smoother potential between the beads than described by the atomistic force field. The faster dynamics can be a problem when the study concerns dynamic properties like the viscosity or the self-diffusion coefficient, but in the present case the speed up of the intermolecular motion helps only to observe an internal conformational changes that otherwise could not be observed.

A similar transition is observed also in dendrimers of higher generations. Figure 7 (top part) shows the time evolution for the λ_i of G3 dendrimers.

In this case, oscillations in the λ_i values are found to correspond again to the *open*/*collapsed* switching. As expected, the oscillation is slower than in G2. The switching is also reflected by the distribution of the λ_2/λ_3 ratio (see Figure 7 bottom part). In this case, the distribution is clearly bimodal.

Figure 8 shows the jumps among the two conformations for the G4: the different global shape is so well-defined because the oscillating period is longer than in the previuos cases. The λ_2/λ_3 distribution shows clearly that the distribution is bimodal.

These results show that, even thought, the CG force field has been devolped from an atomistic simulation that allowed the dendrimers to sample one of global conformational state and a deformation of it, the CG simulations show the switching between the two global states identified as *open* and *collapsed*. This behavior can be explained considering that the global state sampled during the CG simulations (*open*) is a transition state among the two (*collapsed* and *distorted*) found during the atomistic simulation. The CG potential is enough soft to allow the molecule to switch between the three conformations (see Figure 9).

To better relate the CG simulations presented in this paper to the previous atomistic simulations carried out on the isolated dendrimers, we compare the eigenvalues λ_i obtained from the

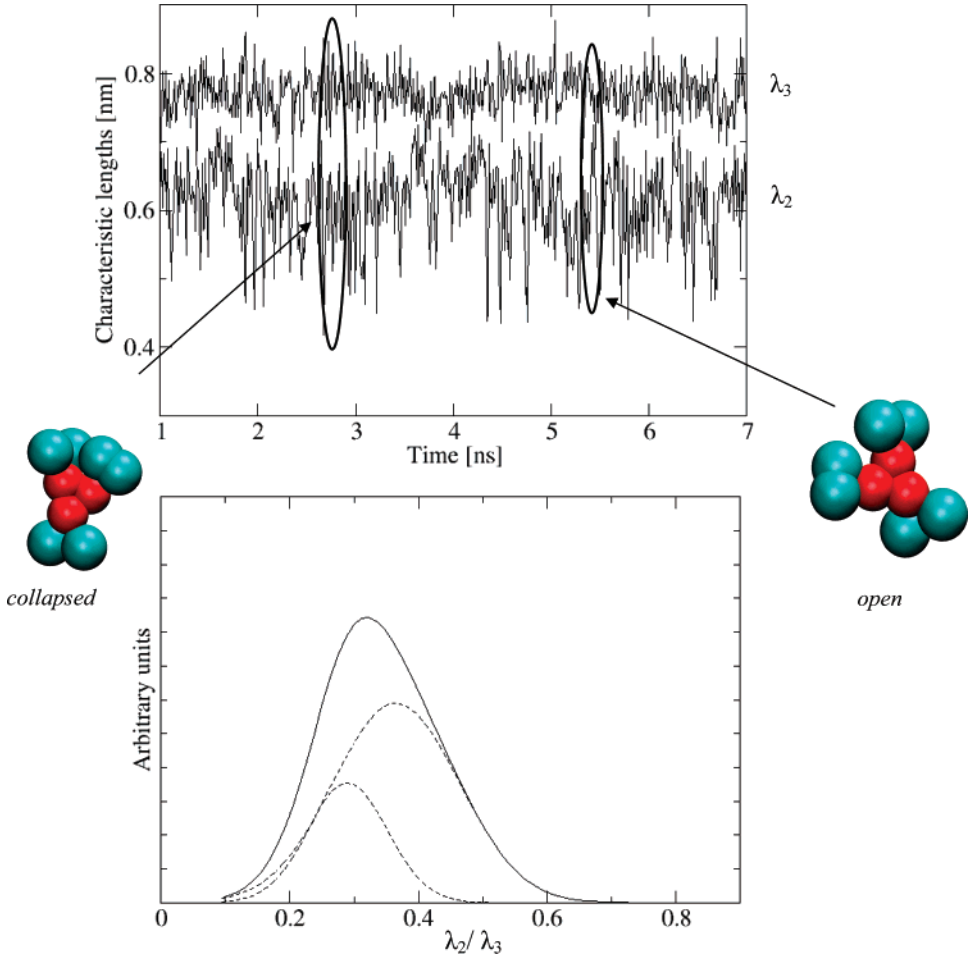

Figure 6. Top: Time evolution of the largest eigenvalues of the gyration tensor for one individual polyphenylene dendrimer of second generation. The two 3D structures (*open* and *collapsed*) corresponding to the different area of the plot, are also reported. Bottom: Distribution of the λ_2/λ_3 ratio (solid line) and corresponding Gaussian distributions fitting the curve (dotted line).

Table 4. Characteristic Lengths λ_1, λ_2, and λ_3 from Atomistic (in Vacuum), Pseudo-CG (Vacuum), and CG (Melt) Simulations of Polyphenylene Dendrimers of Different Generations

generation	$\langle\lambda_1\rangle$	$\langle\lambda_2\rangle$	$\langle\lambda_3\rangle$	$\langle k^2\rangle$
At-G2	3.7 ± 0.4	7.3 ± 0.7	9.0 ± 0.4	$0.173 \pm 5.0 \times 10^{-2}$
pseudo-CG-G2	2.4 ± 0.3	6.0 ± 0.6	7.4 ± 0.3	$0.216 \pm 4.7 \times 10^{-2}$
G2	2.1 ± 0.5	6.1 ± 0.6	7.7 ± 0.4	$0.228 \pm 5.0 \times 10^{-2}$
G3	4.3 ± 0.8	9.2 ± 0.9	11.8 ± 0.7	$0.196 \pm 5.8 \times 10^{-2}$
G4	6.6 ± 1.1	12.3 ± 1.2	15.5 ± 1.0	$0.163 \pm 5.1 \times 10^{-2}$

atomistic G2 to the ones corresponding to the coarse-grained model. It is worth noting that the atomistic bulk simulations and the simulations carried on in vacuum give almost the same eigenvalues. The following comparison is made with the isolated dendrimer only because in this case the molecular switching occurs, and the eigenvalues are the averages of the two conformers *open* and *collapsed*. Then using the atomistic trajectory, we calculate the center of mass of each bead following the coarse-graining scheme used in this paper. In this way we obtain a "coarse-grained" trajectory derived from the atomistic one (we called this model pseudo-CG). On the pseudo-CG trajectory we calculate the eigenvalues λ_i and the anisotropy factor. The shape and mass distribution of the atomistic dendrimer is of course different from the coarse-grained model describing the dendrimer with only nine spheres. The atomistic eigenvalues, indeed, are slightly lager than the pseudo-CG ones, but they have similar ratios. This inaccuracy in describing the real shape of the molecule is also evident comparing the averaged anisotropy factor $\langle k^2\rangle$ of the two models (0.225 and 0.173 respectively) (Table 4). In contrast, a direct comparison among the λ_i of the CG and the pseudo-CG models shows that the values are comparable within their errors.

Inspection of the last column of Table 4 shows that the anisotropy factor $\langle k^2\rangle$ decreases from G2 to G4: for the second generation $\langle k^2\rangle$ is equal to about 0.23, but for higher generation it decreases to a value of 0.163. These trend can be compared with the shape anisotropy factor calculated by Zacharopoulos et al.[17] for a melt of poly(propyleneimine) dendrimers. They found a k^2 of 0.22 for the second generation and a value of around 0.10 for the fifth generation, showing a remarkable decrease with the generations. The authors found, by inspection of several geometrical parameters, that to this change in k^2 corresponds a change in the distribution of the monomers toward a more globular rearrangement. For our rigid dendrimers, this kind of globular rearrangement does not occur and the structure, in spite of a small decrease in k^2, preserves the shape more or less when the generation increases.

Single Molecule Characterization: Hydrodynamic Radius, Structure Factors, and Comparison with Experimental Results. Small-angle neutron scattering experiments (SANS)

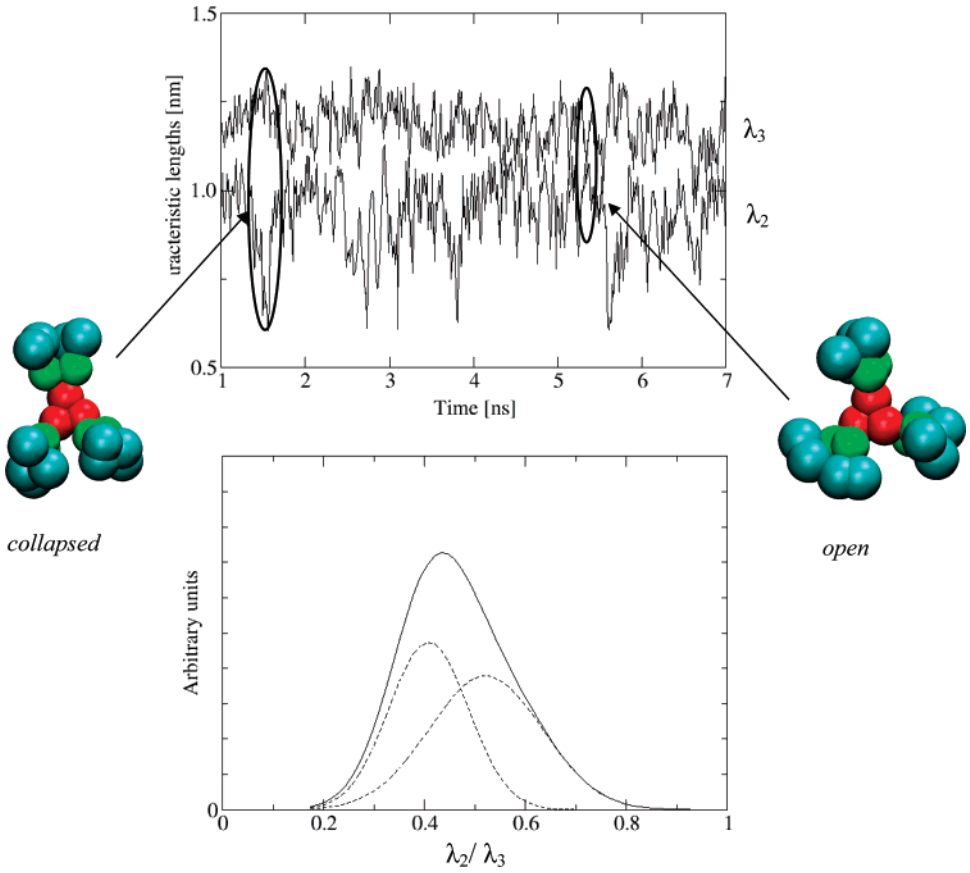

Figure 7. Top: Time evolution of the largest eigenvalues of the gyration tensor for one individual polyphenylene dendrimer of third generation. The two 3D structures (*open* and *collapsed*) corresponding to the different area of the plot, are also reported. Bottom: Distribution of the λ_2/λ_3 ratio (solid line) and corresponding Gaussian distributions fitting the curve (dotted line).

are a suitable analytical method to obtain information on the internal structure and overall shape of dendrimers, such as the hydrodynamic radius (R_H), R_g, and the radial density profile by means of the scattering structure factors.[11] It is possible to calculate the R_H from the simulations, defined as the harmonic mean of the interatomic distances

$$\frac{1}{R_H} = \frac{1}{N^2}\left\langle \sum_{i \neq j} \frac{1}{R_{ij}} \right\rangle$$

where N is the total number of atoms and R_{ij} is the distance between atoms i and j belonging to the same molecule, and the sum is averaged over the MD trajectory. Moreover, the static structure factor $S(q)$ defined as

$$S(q) = \frac{1}{N^2} \sum_{j=1}^{N} \sum_{i=1}^{N} \frac{\sin(qR_{ij})}{qR_{ij}}$$

can be easily calculated from the MD trajectories, too.

In Table 5 (second and third columns), the calculated R_g and R_H are reported for all generations. The available experimental values are reported in the last two columns. For G2 and G3 the corresponding R_H have been measured using the dynamics light scattering on dendrimers with the identical repeat unit, but based on tetra phenyl methane core instead of a single trisubstituted phenyl core, as in our PDs.[29] For G4, SANS experiments have been conducted on the fourth generation PDs with a biphenyl core (4G-biph).[35,36] The extrapolation in the SANS profile to infinite contrast for 4G leads to an experimental R_g of 2.6 nm. All computed values are smaller than the experimental ones. Clearly the chemical nature of the core makes a difference, as discussed in detail in ref 23, and this can account for part of the discrepancy between computed and observed values. We cannot rule out, however, a second contribution to the discrepancy from the underestimation which our coarse-grained model makes describing the atomistic structure (as explained above when we compared the atomistic and the pseudo-CG λ_i). To find an approximate scale factor, which corrects the underestimation by the coarse-grained model, we also calculate R_g for the atomistic model of G2 (1.22 nm), leading to a scaling factor atomistic/coarse-grained dimension of about 1.13. It is worth noting that this scaling factor takes into account only the underestimation of the coarse-grained model and it was not chosen to account for the effect of the dendrimer's core. Indeed, it is known that different dendrimer cores can lead to a different dendrons spatial rearrangement. For instance, Pricl and coworkers[23] found that, for isolated dendrimers the evolution of the structure is intimately related to the dynamics of the core. Despite that they found that the dendrimer core effect on the gyration radius value is evident for small generations in the case of biphenyl core (0.95 nm for the trisubstituted-phenyl-core vs 1.05 nm for the biphenyl core, both second generation dendrimers) and unimportant for the third generation (1.38 nm for both cores). In contrast, the discrepancy is more evident in the case of tetra phenyl methane core, for which they found a value of 1.32 nm for the second generation and 1.78 nm for the third one. We notice, however, that the dendrimer structures found in the present study are remarkably different from those found in ref 23.

The fourth and fifth columns of Table 5 report R_g and R_H values calculated from the CG trajectories and corrected with

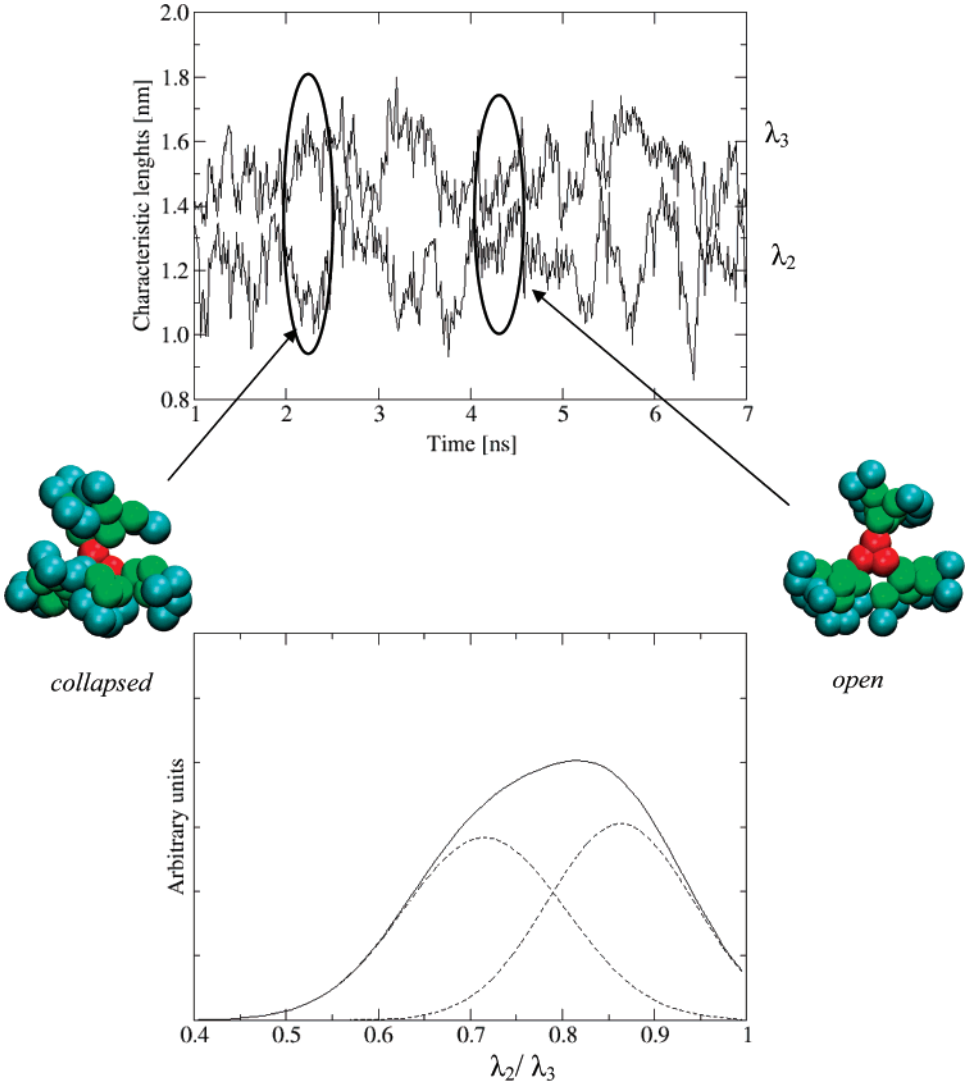

Figure 8. Top: Time evolution of the largest eigenvalues of the gyration tensor for one individual polyphenylene dendrimer of fourth generation. The two 3D structures (*open* and *collapsed*) corresponding to the different area of the plot, are also reported. Bottom: Distribution of the λ_2/λ_3 ratio (solid line) and corresponding Gaussian distributions fitting the curve (dotted line).

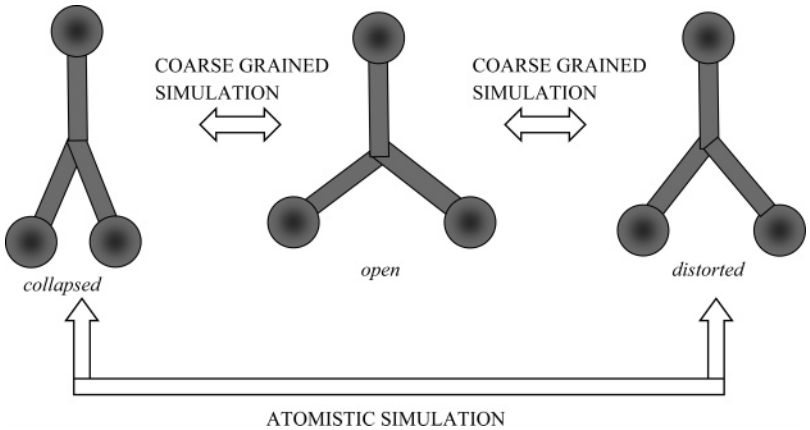

Figure 9. Schematic representations of the global conformations identified during the atomistic and coarse grained simulations. The arrows indicate the conformational changes that occur in the two types of simulation.

the factor described above; these numbers compare well to the experimental values.

Figure 10 shows the structure factor profile for single dendrimer molecules of different generations. For clarity we normalize the plots by the dendrimers' number of beads. All generations have a similar behavior. Moreover, we calculate $S(q)$ for a sphere of radius 2.6 nm (equal to the R_g of G4 PD) and for an ellipsoid with the characteristic lengths of G4. At small q the overlap among the CG and ellipsoid $S(q)$ is very well (Figure 10 bottom part).

The location of the end groups within the dendrimer scaffold is one of the most important properties for the application of dendrimers. PDs are characterized by a stiff structure, which should prevent the terminal group from folding back into the

Table 5. Gyration Radius (R_g) and Hydrodynamic Radius (R_H) for PDs of Different Generation

			theor corrected		expt	
generation	theor R_g [nm]	theor R_H [nm]	R_g [nm]	R_H [nm]	R_g [nm][b]	R_H [nm][a]
G2	1.08 ± 0.3	1.33	1.2	1.5		1.5[a]
G3	1.62 ± 0.6	1.71	1.8	1.9		2.2[a]
G4	2.09 ± 0.8	2.16	2.4	2.4	2.6[b]	

[a] Reference 29. [b] Reference 36.

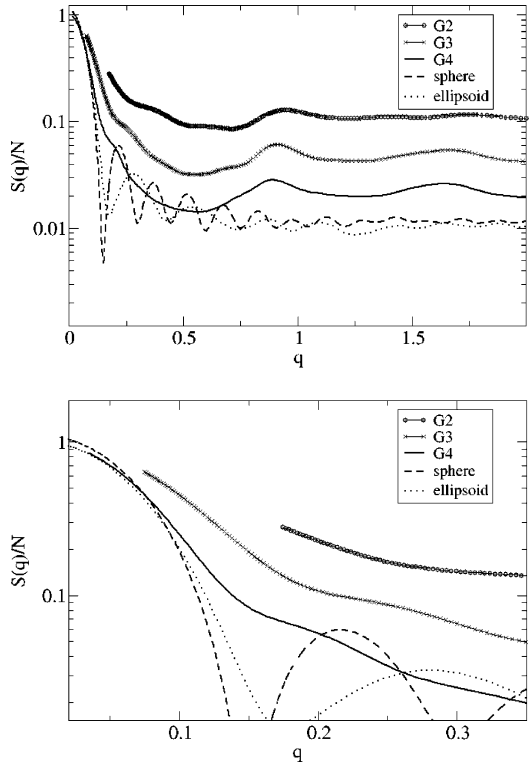

Figure 10. Top: structure factor $S(q)$, normalized with respect to the dendrimer number of beads, for different dendrimer generations. The dotted and dashed lines are relative to the spherical and ellipsoidal model respectively. Below: details of the low wave vector region of the plot, showing the good overlap among the fourth generation and the ellipsoid curve.

interior of the molecule. The spatial arrangement of the dendrons can be evaluated by the calculation of the intra-dendrimer radial distribution function (intra-RDF).

A more detailed vision of the stiffness of the dendrimer branch can be obtaining looking at relative position of the beads within the dendron itself. In Figure 11, we show the intra-dendron RDFs for G3 and G4. To make the plot clear we label the bead A, B_2, B_3, and B_4 depending on which generation they belong to (see the schematic dendrimer representation of Figure 11), and we plot only the intra-dendron-RDF corresponding to the pairs $A-B_2$, $A-B_3$, and $A-B_4$ (the last, of course, only exists for the fourth generation).

The first peak of each graph represents the bond distance between bead of type A and beads of type B directly connected (B_2). The G3 model (top part of Figure 11) does not show any back-folding: the probability of finding a bead belonging to the third generation in the second generation "shell" is zero (i.e., there is no overlap between the first peaks at ca. 0.8 nm and the first peak corresponding to the and groups that lies at 1.2 nm). For the G4 dendrimer (bottom part of Figure 11), there is a small probability to find end beads even at distances smaller than 0.9 nm. This probability is small and the majority of the

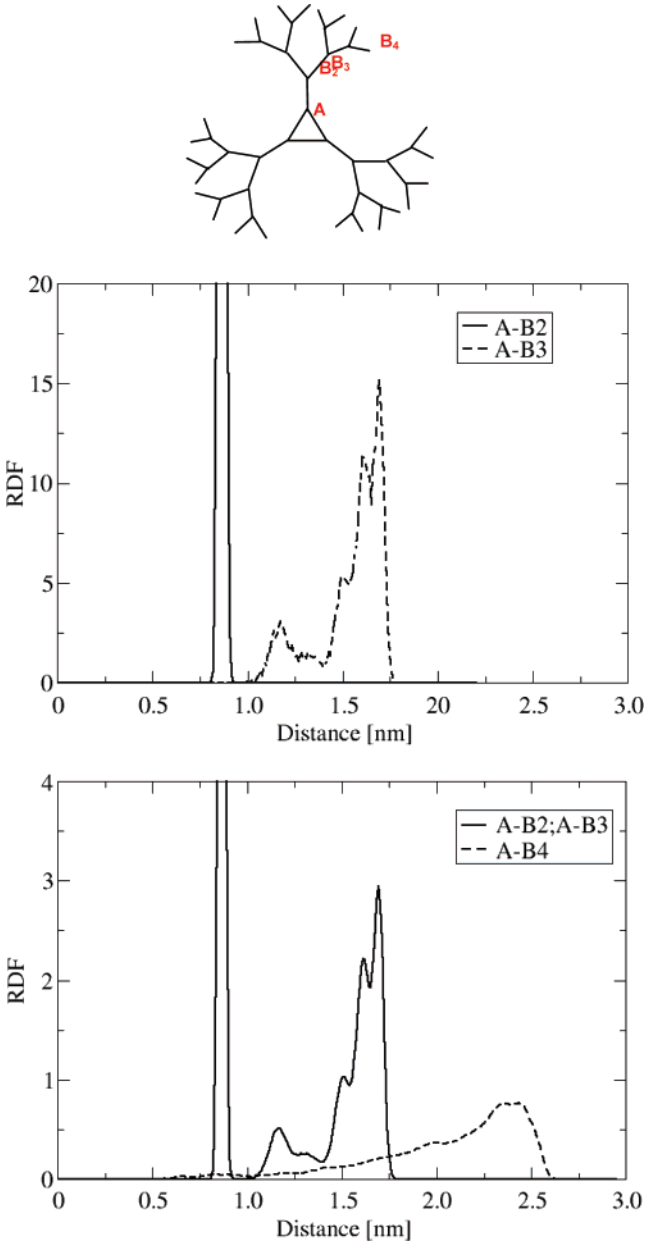

Figure 11. Intramolecular radial distribution functions for polyphenylene dendrimer of third (top) and fourth generation (bottom).

end beads is at a distance beyond 2.4 nm. We conclude that also for the G4 the backfolding is insignificant.

In ref 36, a numerical model is used to fit the experimental SANS results of the fourth generation PDs with a biphenyl core (G4-biph) and from this it has been possible to calculate the average radial bead density $\rho(r)$, defined as the number of beads whose center of mass is located within the spherical shell of radius r and thickness Δr from the center of mass of the dendrimer. This model treats each repeat unit as a sphere, as we did in our coarse-grained description, and it fits the experimental profile. In Figure 12, we report $\rho(r)$ calculated using this numerical model and our CG simulation for the G4 PD. The agreement between the curves is good: in both cases the peaks corresponding to the different generation shell are clearly separated and lie at the same distance r form the dendrimer center of mass, within a small discrepancy due to the different dendrimer cores. In Figure we draw differently the $\rho(r)$ corresponding to the end-beads. In this way the distribution of the end groups inside the dendrimer can be better compared. Using the numerical model, no overlaps occur

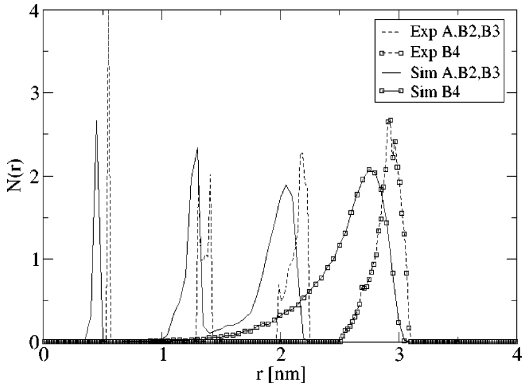

Figure 12. Number of beads located at distance r from the dendrimer center of mass, calculated for a individual polyphenylene dendrimer of generation fourth from coarse-grained simulation (solid line and solid empty square line) and from a numerical model employed to fit SANS experiments[36] (dashed line and dashed empty square line).

between the peaks showing that this model does not find any back-folding. The simulation results confirm the results of the intra-RDF, showing that a small back-folding, on average, can occur in the melt phase. This result can be favorably compared to what reported by Gotze and Likos[37] about their Monte Carlo simulations of concentrated dendrimer solutions. Comparing the $\rho(r)$ calculated for concentrated and dilute solutions, they found that the density profile becomes shorter in range and higher, concluding that the dendrimer shrinks as a results of the increased overall concentration. On the other hand, they found that to this shrinkage does not correspond a sensitive changes in the calculated SANS profile. This leads to the conclusion that dendrimers with the same SANS profile can have a slightly different $\rho(r)$.

5. Summary

In this paper, we have presented a coarse grained model for dendrimer melts, which implicitly contains the chemical details of the atomistic structure. The force field developed is specific to the PDs under investigation (based on a trisubstituted phenyl core), but the coarse-graining procedure can be generalized to all the dendrimers of this type. Bulk systems of polyphenylene dendrimers of second, third and the fourth generation, have been simulated by means coarse-grained molecular dynamics at atmospheric pressure (1 atm) and temperature (323 K) for around 0.1 μs. The simplifications of the coarse-grained model have enabled these large simulation times and, thus, provided the statistical basis for the subsequent analyses. With atomistic models, the results could not have been achieved.

The analysis of the single molecule orientational autocorrelation function shows that the melts are globally relaxed. The order parameter indicates no alignment between the molecules. The computed bulk densities are not due to free volume requirements of the end beads or the intra-dendrimer free volume.

Analyzing the structure of single dendrimer molecules, we have shown that, for all generations, the CG method is able to predict within a small uncertainty the size of the dendrimer. In the CG simulation of the melts, the molecules jump between two global conformational states (*open* and *collapsed*), which were already observed using atomistic MD simulations carried on isolated dendrimer. The switching among the *open* and *collapsed* conformational states can be interpreted as a cooperative phenomenon that involves several degrees of freedom along the dendrons. Unfortunately, the switching frequency cannot be obtained reliably, since coarse-graining speeds up the dynamics artificially. However, we found that the bigger generations have lower switching rates.

Finally, the detailed analysis of the intra-dendron-RDFs and of $\rho(r)$ has shown that our model gives a realistic descriptor of the internal structure of PDs since the peaks are in agreement with SANS experiments. However, even if for these dendrimers in solution a rigid scaffold without back folding of the dendrons was predicted, our results show that in the melt and for high generations there is, a small probability to find end beads at a short distance from the core.

Acknowledgment. We are indebted to Prof. David Brown and Dr. Severine Queyroy of Universite de Savoie for providing the GMQ_num code. We want to thank Dr. Giuseppe Milano for the useful discussions. P. C. thanks the Alexander-von-Humboldt Foundation for a fellowship. F. N. gratefully acknowledges support from FIRB 2001 (Project "Carbon based micro and nanostructures", RBNE019NKS).

References and Notes

(1) Tomalia, D. A.; Frechet, J. M. *Prog. Polym. Sci.* **2005**, *30*, 217−219.
(2) Wang, B.-B.; Zhang, X.; Jia, X.; Chen, Z.; Wei, Y. *J. Polym. Sci., Part A: Polym. Chem.* **2005**, *43*, 5512−5519.
(3) Vicinelli, V.; Ceroni, P.; Maestri, M.; Lazzari, M.; Balzani, V.; Lee, S. K.; van Heyst, J.; Vogtle, F. *Org. Biomol. Chem.* **2004**, *2*, 2207−2213.
(4) Hudson, S. D.; Jung, H. T.; Percec, V.; Cho, W. D.; Johansson, G.; Ungar, G.; Balagurusamy, V. S. K. *Science* **1997**, *278*, 449−452.
(5) Berresheim, A. J.; Muller, M.; Mullen, K. *Chem. Rev.* **1999**, *99*, 1747−1785.
(6) Morgenroth, F.; Reuther, E.; Mullen, K. *Angew. Chem., Int. Ed.* **1997**, *36*, 631−634.
(7) Morgenroth, F.; Berresheim, A. J.; Wagner, M.; Mullen, K. *Chem. Commun.* **1998**, 1139−1140.
(8) Watson, M. D.; Fechtenkotter, A.; Mullen, K. *Chem. Rev.* **2001**, *101*, 1267−1300.
(9) Di Stefano, M.; Negri, F.; Carbone, P.; Mullen, K. *Chem. Phys.* **2005**, *314*, 85−99.
(10) Percec, V.; Ahn, C. H.; Ungar, G.; Yeardley, D. J. P.; Moller, M.; Sheiko, S. S. *Nature (London)* **1998**, *391*, 161−164.
(11) Ballauff, M.; Likos, C. N. *Angew. Chem., Int. Ed.* **2004**, *43*, 2998−3020.
(12) Zook, T. C.; Pickett, G. T. *Phys. Rev. Lett.* **2003**, *90*.
(13) Murat, M.; Grest, G. S. *Macromolecules* **1996**, *29*, 1278−1285.
(14) Lyulin, A. V.; Davies, G. R.; Adolf, D. B. *Macromolecules* **2000**, *33*, 6899−6900.
(15) Freire, J. J.; Rodriguez, E.; Rubio, A. M. *J. Chem. Phys.* **2005**, *123*.
(16) Brocorens, P.; Lazzaroni, R.; Bredas, J. L. *J. Phys. Chem. B* **2005**, *109*, 19897−19907.
(17) Zacharopoulos, N.; Economou, L. G. *Macromolecules* **2002**, *35*, 1814−1821.
(18) Reith, D.; Putz, M.; Muller-Plathe, F. *J. Comput. Chem.* **2003**, *24*, 1624−1636.
(19) Milano, G.; Muller-Plathe, F. *J. Phys. Chem. B* **2005**, *109*, 18609−18619.
(20) Queyroy, S.; Neyertz, S.; Brown, D.; Muller-Plathe, F. *Macromolecules* **2004**, *37*, 7338−7350.
(21) Reith, D.; Muller, B.; Muller-Plathe, F.; Wiegand, S. *J. Chem. Phys.* **2002**, *116*, 9100−9106.
(22) Brocorens, P.; Zojer, E.; Cornil, J.; Shuai, Z.; Leising, G.; Mullen, K.; Bredas, J. L. *Synth. Met.* **1999**, *100*, 141−162.
(23) Pricl, S.; Fermeglia, M.; Ferrone, M.; Asquini, A. *Carbon* **2003**, *41*, 2269−2283.
(24) Carbone, P.; Calabretta, A.; Di Stefano, M.; Negri, F.; Mullen, K. *J. Phys. Chem. A* **2006**, *110*, 2214−2224.
(25) Milano, G.; Goudeau, S.; Muller-Plathe, F. *J. Polym. Sci., Part B: Polym. Phys.* **2005**, *43*, 871−885.
(26) Ponder, J. W. In *TINKER, Software Tools for Molecular Design version 3.8*.
(27) Allinger, N. L.; Yuh, Y. H.; Lii, J. H. *J. Am. Chem. Soc.* **1989**, *111*, 8551−8566.
(28) Brown, D. "The GMQ User Manual Version 3", http://www.univ-savoie.fr/labos/lmops/brown/gmq.html, 1999.
(29) Andreitchenko, E. V.; Clark, C. G.; Bauer, R. E.; Lieser, G.; Mullen, K. *Angew. Chem., Int. Ed.* **2005**, *44*, 6348−6354.
(30) Fox, T. G.; Flory, P. J. *J. Appl. Phys.* **1950**, *21*, 581−591.

(31) Barbieri, A.; Prevosto, D.; Lucchesi, M.; Leporini, D. *J. Phys.-Condens. Mater.* **2004**, *16*, 6609−6618.
(32) Tande, B. M.; Wagner, N. J.; Kim, Y. H. *Macromolecules* **2003**, *36*, 4619−4623.
(33) Loi, S.; Wiesler, U. M.; Butt, H. J.; Mullen, K. *Chem. Commun.* **2000**, 1169−1170.
(34) Depa, P. K.; Maranas, J. K. *J. Chem. Phys.* **2005**, *123*.
(35) Rosenfeldt, S.; Dingenouts, N.; Potschke, D.; Ballauff, M.; Berresheim, A. J.; Mullen, K.; Lindner, P. *Angew. Chem., Int. Ed.* **2004**, *43*, 109−112.
(36) Rosenfeldt, S.; Dingenouts, N.; Potschke, D.; Ballauff, M.; Berresheim, A. J.; Mullen, K.; Lindner, P.; Saalwachter, K. *J. Lumin.* **2005**, *111*, 225−238.
(37) Gotze, I. O.; Likos, C. N. *J. Phys.: Condens. Matter* **2005**, *17*.
(38) Rosenfeldt, S.; N. Dingenouts, D. Potschke, M. Ballauff, A. J. Berresheim, K. Muellen, P. Lindner. *Angew. Chem., Int. Ed.* **2004**, *43*, 109.

MA071001F